A fundamental study of the flow past a circular cylinder using Abaqus/CFD

Masami Sato, and Takaya Kobayashi

Mechanical Design & Analysis Corporation

Abstract: The latest release of Abaqus version 6.10 includes Abaqus/CFD. The inclusion of this software makes it possible for users to perform a fluid analysis in a more user-friendly manner. Independent single software solely for CFD is currently available from many developers, and many attempts have been made to link software of CFD to structural analysis system using some specific procedures such as fluid structure interfaces (FSI). Direct implementation of CFD in FE structural analysis software offers ease of access to CFD. Adopting the position of a mechanical engineer trying to use CFD for the first time, a series of fundamental analyses were performed using Abaqus/CFD. Fluid flow around a circular cylinder placed in a uniform flow was investigated in addition to the occurrence of various phenomena associated with von Karman vortices and the oscillation of a circular cylinder excited by these vortices over the object.

Keywords: Abaqus/CFD, wake flow, von Karman vortices

1. Introduction

We have studied the fluid dynamics in basic engineering education. However, it is not particularly easy to apply knowledge of fluid dynamics in to actual designs. In practice, although structural mechanics may appear in every aspect of the design process, it is very rare for fluid dynamics to be present in the apparent in the original equations. In many cases, fluid flow is translated using particular design formulae. Pressure drop calculations in a pipe line or the calculation of the heat transfer coefficient are examples of typical formula-based design.

The environment contains a multitude of various fluids. Accordingly, there are plenty of objects to which fluid dynamics can be applied. However, not only are fluid flows not visible, it is very difficult to understand the following behaviors of fluids:

- **i.** Fluid is significantly deformable compared with solids, and the degree of deformability depends upon the viscosity of the fluid.
- **ii.** The interaction of a fluid flow with a solid surface is important subjects. More specifically, the attachment to a solid surface, the development of a boundary layer, and the separation.
- **iii.** In addition to these phenomena, the transition of laminar flow to turbulent flow occurs.

These properties of fluid flow make it difficult to apply fluid dynamics in practice. Abaqus is considered to be the best option for general purpose nonlinear FEM, and the latest version includes Abaqus/CFD. Abaqus/CFD is a brand new program developed within the Abaqus system,

and it offers the user a rather different but a much-improved environment from that available with existing CFD software only. Abaqus/CFD is more user-friendly and easily accessible and can be expected to find uses in coupled fluid-structure analysis.

Again, considering the role of fluid dynamics, the role can be categorized into the following three functions:

(a) to understand actual fluid motion ;

(b) to identify the fluid motion induced force acting on an object immersed in a fluid;

(c) to determine how an object moving in a fluid and subjected to fluid-induced force changes its motion and how such a moving object, in turn, simultaneously causes a change in the motion of fluid.

In terms of utilizing CFD in turbulence modeling or in development new analytical approach , such as the particle method, (a) is very important. In addition to comprehensively deal with the fluid-structure coupling problem, it is important to address (c). However, in relation to common aspects of mechanical design, (b) is the best target for exploiting CFD.

In general, textbook on fluid mechanics provide examples fluid flow around a circular cylinder as basic problems. Taking such a problem, the fluid-induced force acting on a circular cylinder immersed in a uniform flow is estimated. However, the problem is addressed not in a single chapter, but over several chapters. For example, a chapter on ideal fluids may describe the D'Alembert's paradox and periodical characteristics of the von Karman vortices, and another chapter on viscous flows then describes the separation of boundary layers. The relationship between momentum and drag is elaborated upon a chapter of its association with the formation of wake.

As a result, it is almost impossible to develop a comprehensive understanding of the above-mentioned behaviors and characteristics of fluid flow based on the knowledge in university textbooks. If CFD is used following proper guidance in appropriate tutorials, it will be possible for a mechanical engineer to analyze the problem of fluid flow around a circular cylinder with relative ease. Implementing CFD into structural engineering software may open a new way toward understanding complicated fluid flow behaviors, something that would substantially benefit many engineers.

We performed a series of analyses in which fluid flow around a circular cylinder immersed in a uniform flow was used to trace the occurrence of von Karman vortices and to determine the resultant vibration of the cylinder.

2. Unsteady state flow around a circular cylinder immersed in a uniform flow

The following Navier-Stokes equation of the motion of fluid with incompressible viscous flow is used; this equation indicates that the inertia force, pressure, and viscous force are in equilibrium.

$$\rho \frac{D\boldsymbol{u}}{Dt} = -\operatorname{grad} p + \mu \Delta \boldsymbol{u} \tag{1}$$

[inertia force] [pressure] [viscous force]

where ρ is the density, $\boldsymbol{u}$ is the velocity vector, t is the time, p is the pressure, and μ is the coefficient of the viscosity.

Fluid flow analysis aims to determine the relationship between pressure and flow velocity by solving Equation 1, which is subject to a geometric boundary condition, i.e., the interface surface at which a fluid contacts a solid object. As very small uneven roughness is unavoidably distributed over the whole surface of a solid object, fluid particles are completely captured on the solid surface due to the viscosity of the fluid. This property of fluids leads to a very important assumption such that a condition of zero fluid velocity (i.e., no slip) is achieved over the whole surface of a solid object.

The relative importance of the ratio of the inertial forces to the viscous forces for the flow conditions is quantified by taking L as the characteristic scale of flow and U as characteristic velocity of flow; $D/Dt \approx L/U$, $\Delta \approx 1/L^2$ can then be introduced, and the index yields:

$$\frac{[\text{inertia force}]}{[\text{viscous force}]} = \frac{\rho \dfrac{U}{L/U}}{\mu \dfrac{U}{L^2}} = \frac{\rho UL}{\mu} = Re \tag{2}$$

where Re represents a dimensionless number called the Reynolds number. If the Navier-Stokes Equation 1 is converted to a dimensionless form, it is well known that this dimensionless equation depends on only the Reynolds number. Thus, if Reynolds numbers are identical, an overall field containing every individual flow with a geometrically similar boundary shape to each other can be regarded as being similar overall. In addition to increasing velocity, a greater density, a smaller viscosity, or a larger solid body size tend to increase the Reynolds number, thereby equally affecting the overall flow field. Accordingly, it can be said that the Reynolds number represents a dimensionless flow velocity.

Flow patterns generated around a circular cylinder immersed in a uniform flow are shown in Figure 1 (Hughes & Brighton, 1999). In relation to the flow around an object, a combination of a uniform flow with a circular cylinder will be the simplest case. The pattern of this flow varies depending upon the Reynolds number.

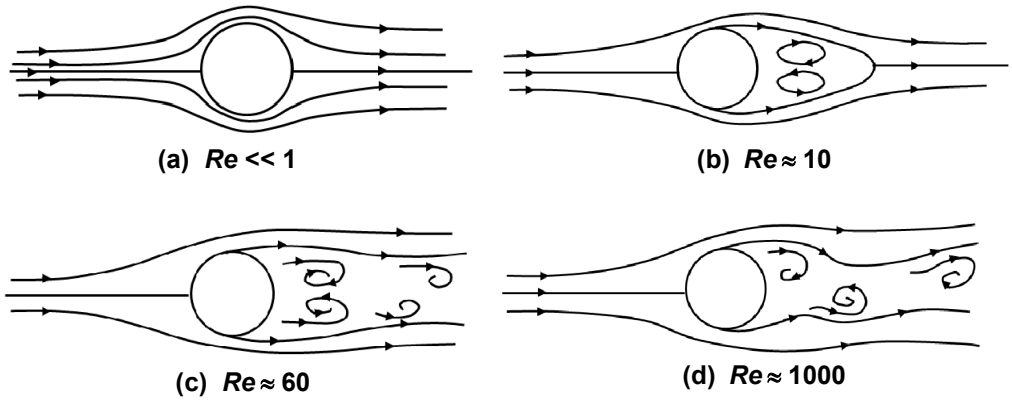

Figure 1. Flow pattern generated around a circular cylinder

Figure 1-(a) shows a flow with a very small Reynolds number. The shape of every streamline is symmetrical not only around the cylinder's upper to lower side, but also around its front to rear. As the Reynolds number increases, the front to rear symmetry disappears, and the interval of the streamlines of the cylinder's rear flow widens. As the Reynolds number reaches close to 10, a closed region of the streamline is generated within the cylinder's rear flow. The fluid in the upper half of this region rotates clockwise, and the fluid in the lower half rotates counter clockwise. This phenomenon is the result of the so-called generation of vortices. Figure 1-(b) depicts this state.

As the Reynolds number increases, the length of the vortex increases. When the Reynolds number exceeds 60, the rear flow becomes unstable as shown in Figure 1-(c), and the vortex begins to oscillate in an up-down direction. The fully formed vortex is carried away on the surrounding main flow, and a vortex subsequently occurs on the other side. This vortex then expands before finally dissipating and departing leaving the circular cylinder. In addition to this flow process, every pair of upper and lower vortices behind the cylinder is stored in an alternative regular array to form twin rows of vortices. These rows are called the von Karman vortex street. While the main flow approaching the circular cylinder is in a uniformly steady state, a periodically varying flow characteristic of the von Karman vortex street appears in the cylinder's rear flow.

As shown in Figure 1-(d), as the Reynolds number reaches 1,000, the vortices are mixed together, and the flow behind the cylinder (wake) behaves very irregularly in time and space scale. This behavior is the so-called state of turbulent flow. However, a free stream distant from the wake region maintains a steady state, and the streamlines are held in a regular and smooth shape. This phenomenon is known as laminar flow.

Abaqus/CFD was used in this study to perform analyses, within a range of Reynolds numbers up to 200 under which we considered it possible to analyze the occurrence of laminar flows.

3. Analysis model

The analysis model in this study is shown in Figure 2. The fluid was assumed to be water at 293 K where the density was $\rho = 998.204$ (kg/m^3) and the coefficient of viscosity was $\mu = 1.002 \times 10^{-3}$ (Pa sec). The diameter of the cylinder was assumed to be d = 8 mm. Naturally, an analysis of the von Karman vortex should begin with two-dimensional behaviors of the flow around the circular cylinder. However, as, Abaqus/CFD is designed to deal with fluids with three-dimensional behaviors, the fluid was modeled using the three-dimensional element (FC3D8), which has one division and a thickness of 1 mm.

There has been much discussion of extending the analysis region. We employed a region with a dimension of 50 mm in the flow direction, 150 mm in the outflow direction, and 100 mm in the lateral direction measured from the center of the cylinder. We followed suggestions outlined in recent research on how to achieve more than 5 d in the inflow direction, more than 15 d in the outflow direction, and more than 10 d in the lateral direction (Zdravkovich, 1997).

If one or more von Karman vortices occur, the way in which these vortices are discharged from the analysis region is a problem. That is, it is very important to specify the necessary conditions to avoid going back to front flow as a result of wake discharging in the analysis model. For example, it may be possible to diffuse the vortices artificially and stabilize their discharge by gradually increasing the size of the mesh toward the rear flow direction. However, in practice, we employed homogeneous meshing.

In addition, the flow channel is narrowed due to the existence of the circular cylinder, with the result that the fluid flow is locally accelerated. Due to this acceleration, the estimated drag on the object can be expected to be greater than the actual drag.

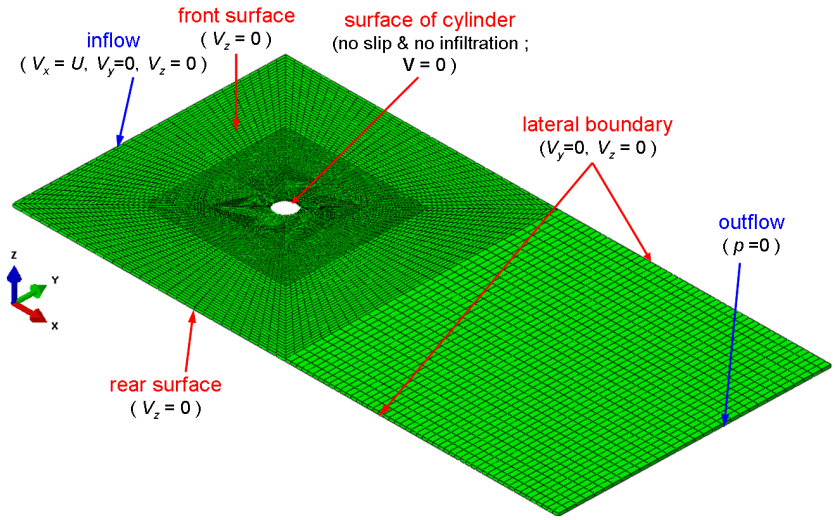

Figure 2. Analysis model and boundary conditions

3.1 Boundary conditions

To obtain the two-dimensional behaviors of the fluid, a zero component of the velocity in the z-direction was assigned to both the front and the rear surfaces. At the lateral boundary of the model, the velocity in the x-direction was not specified, whereas the zero component of the velocity in y-direction was intended to suppress the occurrence of any lateral outflow. This boundary condition is so-called free slip condition. In addition, the boundary condition on the surface of the cylinder was assumed to be a non slip condition. Thus, all the components of the velocity were set to zero. This boundary condition is a fluid that is attached to a wall surface.

As Abaqus requires that the boundary condition specifying some degree of pressure should be given in the model, because Abaqus adopts the decoupled method to solve the Navier-Stokes equation. So, zero pressure was applied to the outflow boundary in this analysis.

On the inflow boundary, a uniform velocity was assigned to the x-direction. The inflow velocity may be obtained based on the Reynolds number using Equation 2. The characteristic length of linear dimension of flow in Equation 2 is given as the diameter *d* in the case of the flow around the circular cylinder. Table 1 provides information on all of the conditions used to observe variation in the flow field associated with different Reynolds numbers.

Table 1. Inflow velocity at each Reynolds number

	***Re* (-)**	***U* (mm/sec)**		***Re* (-)**	***U* (mm/sec)**
CASE1	0.038	4.77×10^{-3}	**CASE5**	26	3.26
CASE2	0.1	1.25×10^{-2}	**CASE6**	50	6.27
CASE3	1.1	0.138	**CASE7**	100	12.5
CASE4	20	2.510	**CASE8**	195	24.5

(A water temperature of 293 K was assumed: $Re = \rho UL / \mu$)

4. Analysis results

4.1 Variation in flow patterns corresponding to various Reynolds number

Using a dual-core CPU, the analysis of CASE1 took about 60 sec. The time taken to perform the analysis duration increased with an increase in the Reynolds number, with the analysis of CASE8 taking about 8,000 sec.

Streamlines derived from the analysis are shown in Figure 3. Some typical cases compared with the experimental results (Van Dyke, 1982; JSME, 1992) are shown in Figure 4.

CASE1 and CASE2 correspond to flows with a sufficiently low Reynolds number (slow flow), and their streamlines appear symmetrically, front to rear. When the Reynolds number exceeded 1, as seen in CASE3, the symmetry was lost in the front and rear flows. However, no separation of fluid flow occurred. CASE4 to CASE6 correspond to a Reynolds number in the range of 20 to 50, and a pair of upper and lower vortices was generated within the wake of the cylinder. As the Reynolds number increased, the vortex region expanded and increased in length.

In CASE6 and CASE7 where the Reynolds number exceeded 100, the von Karman vortex street occurred. When the Reynolds number was higher, the von Karman vortices lasted for a shorter a period. As a result, the distance between the vortices decreased. As shown in Figure 4, the results of the analysis are in good agreement with the visualized outcome derived from the experiments.

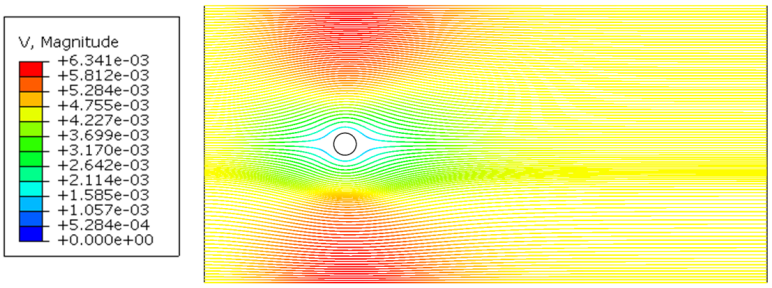

(a) CASE1 *Re* = 0.038

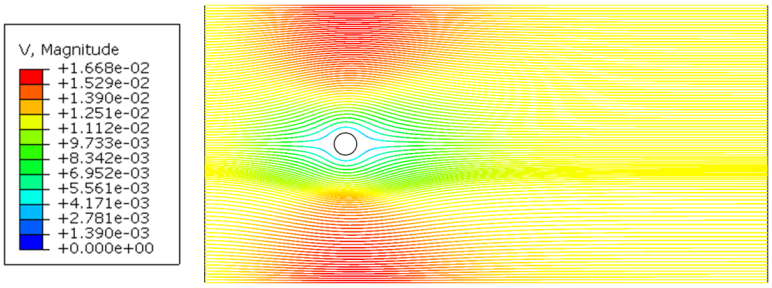

(b) CASE2 *Re* = 0.1

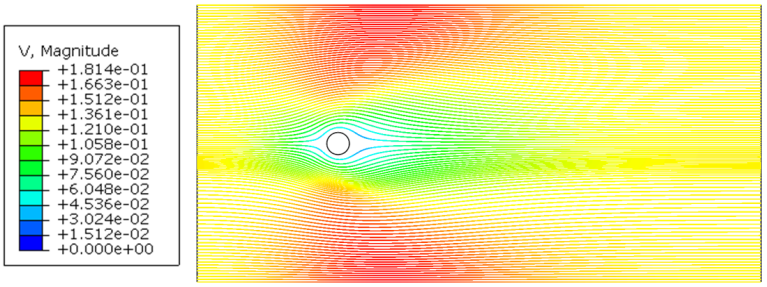

(c) CASE3 *Re* = 1.1

Figure 3. Results of the analysis of streamline patterns

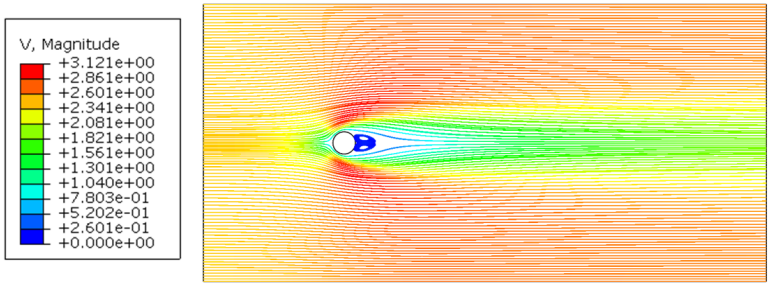

(d) CASE4 *Re* = 20

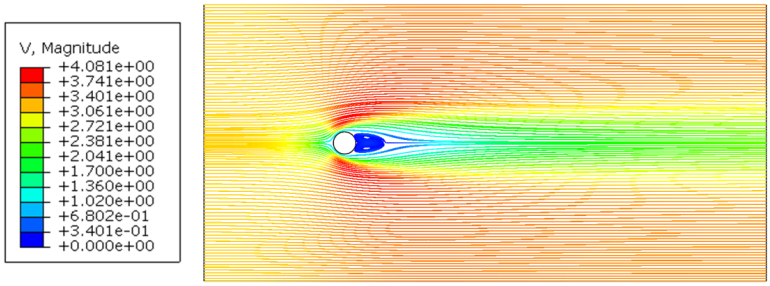

(e) CASE5 *Re* = 26

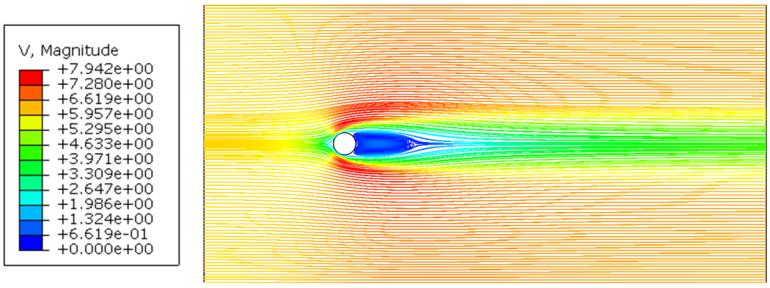

(f) CASE6 *Re* = 50

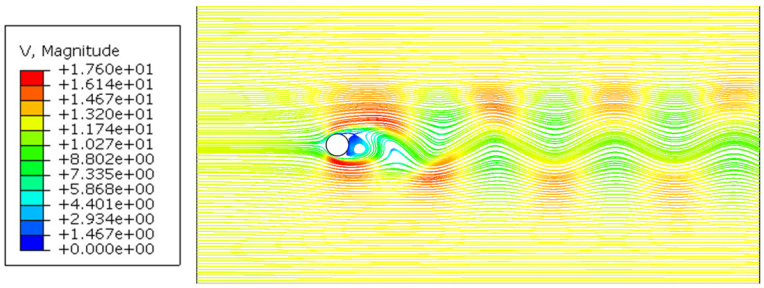

(g) CASE7 *Re* = 100

Figure 3 (cont). Results of the analysis of streamline patterns

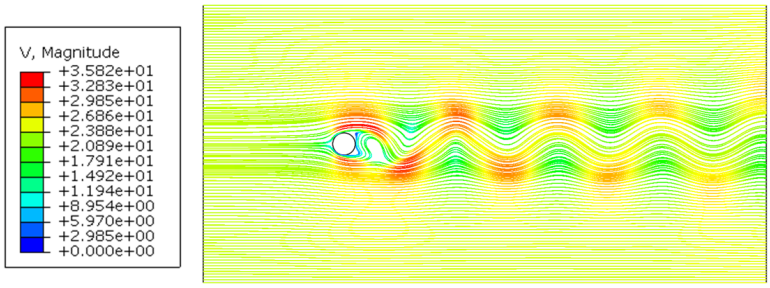

(h) CASE8 *Re* = 195

Figure 3 (cont). Results of the analysis of streamline patterns

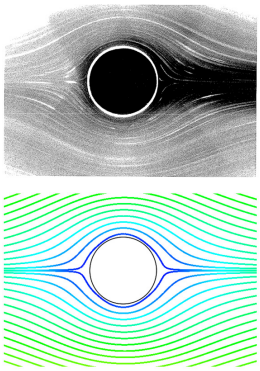

(a) CASE1 *Re* = 0.038

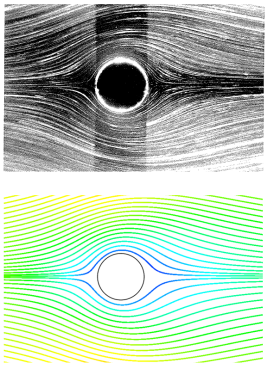

(b) CASE3 *Re* = 1.1

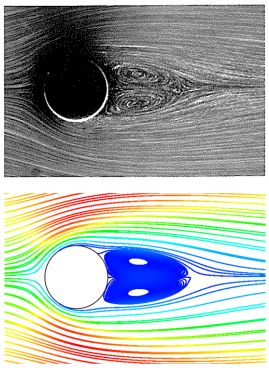

(c) CASE5 *Re* = 26

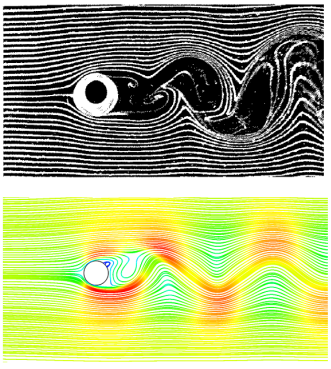

(d) CASE8 *Re* = 195

Figure 4. Comparison between the results of the analysis and the experimental data

(upper : experimental results; lower : analysis results. Note: the steaklines in CASE8.)

4.2 Estimation of flow separation

Taking CASE6 (Reynolds number, Re=50) as an example, the behavior of the separation of the flow was traced. The distributions of the velocity vectors in the vicinity of the cylinder are plotted in Figure 5. Measuring the angle clockwise starting from the center of the front edge of the cylinder, it was found that the flow begins to separate from the wall surface at an angle of about 130 deg and that reverse flow region formed.

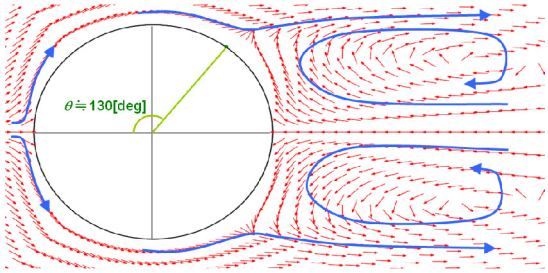

Figure 5. Flow velocity vector in the vicinity of the cylinder

Figure 6 shows the distributions of the velocities (velocity measured at 0.1 mm from the surface), pressures and wall shear stress at $\theta = 0 \sim 180$ deg on the cylinder surface. As the stagnation point is situated at the front edge of the cylinder, the velocity was zero. The velocity of the cylinder's front flow accelerated, whereas the velocity of the rear flow decreased. According to Bernoulli's principle, there is a certain relationship between flow velocity and pressure, with increasing flow velocity resulting decreasing pressure. The resultant pressure distributions conformed to this principle.

As the flows moved down-stream and their respective velocities were gradually reduced due to the effects of viscosity and the pressure gradient, the flow can no longer travel along the surface of the cylinder. This phenomenon is called the separation point, which is the point at which the flow is separated from the cylinder's surface. In Figure 6, the point location $\theta \approx 130$ deg corresponds to the separation point at which the wall's shear stress became zero.

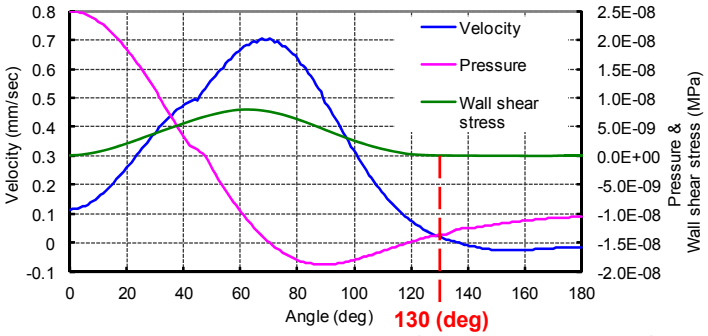

Figure 6. Velocity on the cylinder's surface, distribution of pressure, and the wall's shear stress

4.3 Estimation of fluid force

In Abaqus version 6.11, a time history of the fluid force acting on an object can be generated for a specified fluid surface. Using this feature, the coefficients of drag on the cylinder surface are estimated, and the results of the analysis are verified with the estimated drag.

As drag is a component of the force parallel to the direction of a uniform flow, the x-component of fluid force acting on the surface, F_x, was used in this analysis. This drag, F_x, associated with the coefficient of drag, C_D, is shown in the following expression.

$$C_D = \frac{2F_x}{\rho U^2 S} \tag{3}$$

where S is a reference area that corresponds to a projected area onto the surface of a cylinder that is perpendicular to the flow. In this analysis, a projected area was obtained by multiplying the diameter by the thickness, i.e., $S = 1 \times 8 = 8$ mm^2.

In this verification, the focus was on steady state flow. However, the analysis was unsteady state flow. So the analysis of unsteady state flow should be carried out starting from time zero and proceeding until a steady state flow is reached. Typical cases of the time history of fluid force generated on the cylinder are shown in Figure 7. With a lower Reynolds number, the fluid force simply reaches stationary state, whereas in the presence of the von Karman vortices, the fluid force was observed on one occasion to decrease substantially and then return to a stationary state. However, as the vortices occurred periodically, the fluid force was superimposed by higher harmonics.

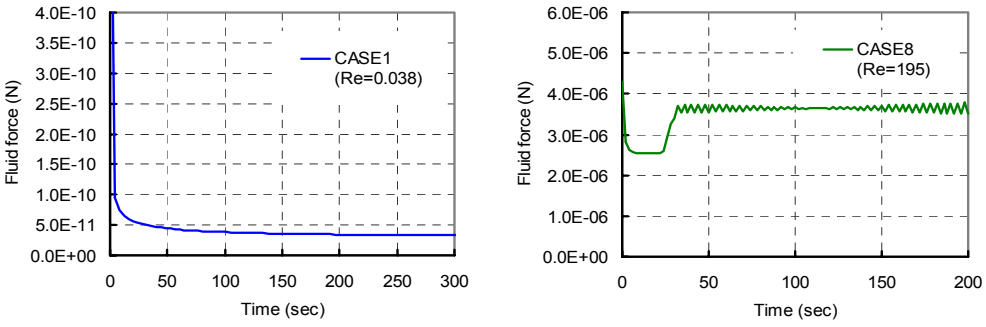

(a) CASE1 *Re* = 0.038 **(b) CASE8 *Re* = 195**

Figure 7. Time history curves of fluid force (CASE1, CASE8)

The drag coefficients in each analysis calculated using Equation 3, the drag coefficients obtained from the experiments (Hughes and Brighton, 1999), and the results obtained using the Oseen approximation (Equation 4) by Lamb are shown together in Figure 8.

$$C_D = \frac{8\pi}{Re(2.002 - \ln Re)} \tag{4}$$

The results of the analysis generally yielded rather higher values of the coefficients of drag than those obtained in the experiments. However, shapes of the curves were found to be approximately the same. The difference between the coefficients of drag in the analysis and the experiments is likely due to local acceleration caused by the lateral analysis region being finite.

Furthermore, if the Reynolds number becomes higher than 200, three-dimensional characteristics of the von Karman vortices may appear, and then flow will be transitioned into a turbulent flow. These phenomena will be addressed in a future study.

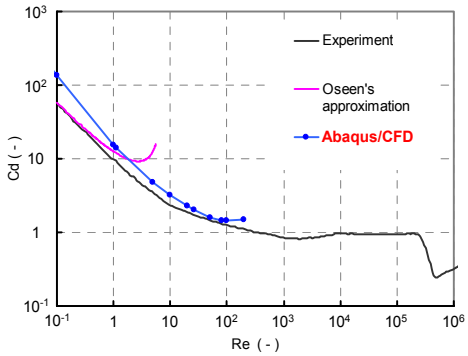

Figure 8. Variation in the coefficient of drag with various Reynolds numbers

4.4 Estimation of Strouhal number

Then, we tried to estimate the frequency of the von Karman vortices, which were generated behind the circular cylinder. It is known that the frequency of the vortices plural *f* can be converted to a dimensionless number using the following expression

$$S_t = \frac{f \times L}{U} \tag{5}$$

This dimensionless number is called the Strouhal number (S_t). Figure 9 shows curves for various Strouhal numbers vs. those for various Reynolds numbers obtained from the analysis, as well as, those measured in earlier the experiments (Zdravkovich, 1997), those approximated using Equation 6 established by Rayleigh, and those derived from Equation 7 formulated by Roshko. The results of the analysis were found to be mostly coincident with the theoretically or experimentally derived curves.

$$S_t = 0.195 \times \left(1 - \frac{20.1}{Re}\right) \tag{6}$$

$$S_t = 0.212 \times \left(1 - \frac{21.1}{Re}\right) \tag{7}$$

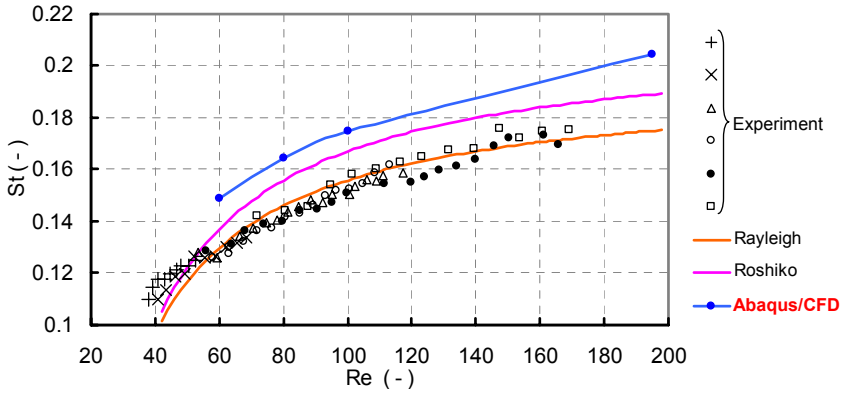

Figure 9. Variation in the Strouhal number vs. various Reynolds numbers

5. Fluid-structure coupling problem

In the final stage, a fluid-structure coupling problem was analyzed. In the problems considered earlier, the circular cylinder was assumed to be stationary in a flow. This assumption was changed, with the circular cylinder now supported by a spring in the vertical direction (i.e., normal to the flow direction). In response to this change, the vibration of the circular cylinder would be expected to be excited due to the occurrence of von Karman vortices. This circular cylinder was modeled using tetrahedral stress/displacement elements (C3D8R) and connected with springs in the y-direction while kept stationary in the x-direction. The material constants of the cylinder were defined as: density $\rho = 7{,}850$ kg/m^3, Young's modulus $E = 2.0 \times 10^5$ MPa, and Poisson's ratio $\nu = 0.3$, nevertheless, the cylinder behaved as rigid body. The values employed in Section 3 were applied to the fluid's material constants as: velocity U=12.5 mm/sec; Reynolds number Re=100. The natural frequency f_n of the spring can be expressed by the following formula, where k denotes the spring constant of the spring and m is the mass of the cylinder

$$f_n = \frac{1}{2\pi}\sqrt{\frac{k}{m}} \tag{8}$$

This natural frequency does not include the effect from the added mass by the fluid. The Strouhal number S_{tn} in respect of this natural frequency is defined by the formula

$$S_{tn} = \frac{1}{2\pi}\frac{U}{f_n D} \tag{9}$$

In this analysis, although the flow rate was kept constant, the Strouhal number was varied by changing the spring constant. Values shown in Table 2 were applied to the spring constants of the spring. Ideally, the effect from the Reynolds number should be examined with changing flow rate, but this effect should be studied at a later stage.

Table 2. Spring constant for each Strouhal number

	S_{tn} (-)	k (N/mm)		S_{tn} (-)	k (N/m)
CASE1	0.7	1.98×10^{-6}	**CASE4**	1.0	9.71×10^{-7}
CASE2	0.8	1.52×10^{-6}	**CASE5**	1.1	8.02×10^{-7}
CASE3	0.9	1.20×10^{-6}	**CASE6**	1.2	6.74×10^{-7}

The Strouhal numbers S_{tn} vs. the vibration frequencies of the cylinder are plotted in Figure 10. Figure 11 shows the vibration amplitudes Y of the cylinder vs. the various Strouhal numbers S_{tn}. In both of these figures experimental results (Hartlen, 1970) and our analytical results are plotted.

As clearly noted in Figure 10, a lock-in phenomenon is observed in the experimental results within a range of S_{tn} = 0.8~1.15, which indicates the existence of a specific region where vibration frequencies of the cylinder remain mostly in a similar range. However, it was not possible to visualize this lock-in phenomenon in this analysis. Therefore, the results show a tendency of monotonous increase in the vibration frequencies of the cylinder in accordance with an increase in the Strouhal number. If a cylinder is excited by von Karman vortices, it is likely that locally three-dimensional flow in the vicinity of the cylinder might occur. However, the model in our analysis was not capable of tracing such phenomena.

In addition, as seen in Figure 11, the vibration amplitudes of the cylinder sharply increased in the lock-in region, something that would lead to a high possibility of the flow transitioning into turbulent flow. This study was largely limited to laminar flow; the possibility of turbulent flow should be investigated in future studies.

6. Conclusion

Taking fluid flows generated around a circular cylinder immersed in a uniform flow as an object of study, a series of analyses using Abaqus/CFD were performed for a specific region with Reynolds numbers up to 200. The results were found to be in good agreement with those of earlier experiments. As a consequence, we have obtained comprehensive knowledge and findings that can be applied to problems associated with fundamental estimation of the flow around the circular cylinder. Although we verified the basic capabilities of Abaqus/CFD with regard to coupled structural fluid analysis in this study, additional analyses are needed to verify more advanced features of the software.

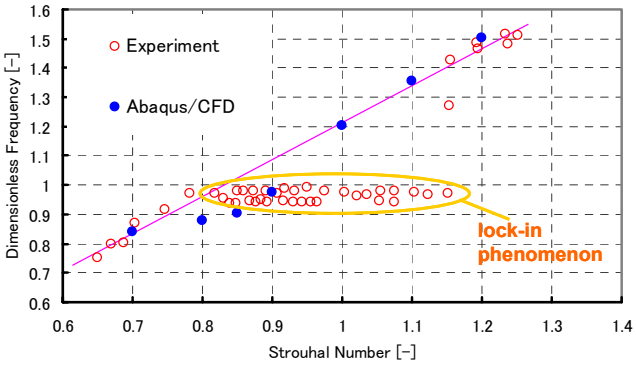

Figure 10. Variation in the vibration frequencies corresponding to each Strouhal number

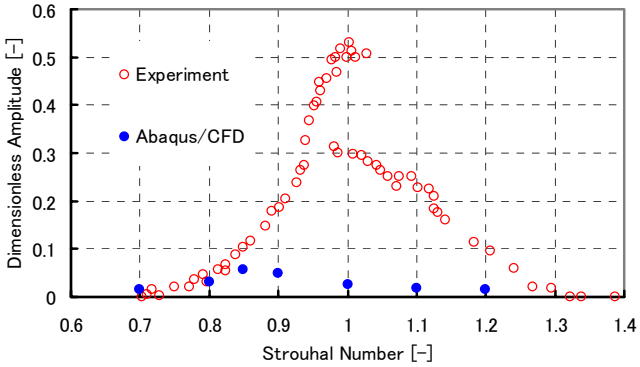

Figure 11. Variation in the vibration amplitudes corresponding to each Strouhal number

7. References

1. Hughes, W.F., & Brighton, J.A., "Schaum's outline of fluid dynamics," USA: McGraw-Hill, p.102, 1999.
2. Van Dyke, M., "An album of fluid motion," USA: The Parabolid Press, p.28, 1982
3. The Japan Society of Mechanical Engineers. "Photograph collection of Flow," JPN: Maruzen Company, pp.2-5, 1992.
4. Zdravkovich, M.M., "Flow around circular cylinders, Vol.1: Fundamentals," USA: Oxford University Press USA, p.61, pp.258-259, 1997.
5. Hartlen, R.T., & Currie, I.G., "Lift-oscillator model of vortex-induced vibration," Proc. ASCE, J. Eng. Mech. Div, Vol.96, No.5, pp.577-591, 1970